sustainability

MDPI

Article

Thermal and Optical Analyses of a Hybrid Solar Photovoltaic/Thermal (PV/T) Collector with Asymmetric Reflector: Numerical Modeling and Validation with Experimental Results

Dimitrios N. Korres, Theodoros Papingiotis, Irene Koronaki * and Christos Tzivanidis

School of Mechanical Engineering, National Technical University of Athens, 157 73 Athens, Greece; korres@central.ntua.gr (D.N.K.); thpapingiotis@mail.ntua.gr (T.P.); ctzivan@central.ntua.gr (C.T.)
* Correspondence: koronaki@central.ntua.gr

Abstract: This study presents a combined thermal and optical, three-dimensional analysis of an asymmetric compound parabolic collector (ACPC) with an integrated hybrid photovoltaic/thermal (PV/T) receiver with the aim of establishing a sustainable approach in two ways: firstly, by determining the optimal tilt angle for operations, and secondly, by introducing an innovative simulation method which reduces computational cost while calculating thermal performance. Initially the Incident Angle Modifier (IAM) was calculated for a wide range of incident angles, and the ray-tracing results were verified using three different simulation tools (Tonatiuh, COMSOL, and SolidWorks) with mean deviations being lower than 4%. The optimal tilt angle of the collector was determined for seven months of the year by conducting a detailed ray-tracing analysis for the mean day of each month considering whole day operation. In the thermal analysis part, the authors introduced novel numerical modeling for numerical simulations. This modeling method, designed with sustainability in mind, enables lighter computational domains for the air gap while achieving accurate numerical results. The approach was established using two distinct simulation tools: COMSOL and SolidWorks. From the optical analysis, it was found that in all months examined there is a four-hour time range around solar noon in which the optimum tilt angle remains constant at a value of 30°. The numerical models constructed for the thermal analysis were verified with each other (6.15% mean deviation) and validated through experimental results taken from the literature regarding the examined collector (<6% mean deviation). In addition, the two simulation tools exhibited a deviation of around 6% between each other. Finally, the thermal performance of the collector was investigated for the mean day of September at solar noon by adopting the optimal tilt angle for that month according to the optical analysis, considering inlet temperatures from 20 °C up to 80 °C.

Keywords: hybrid solar PV/T; asymmetric reflector; new modeling method; optical simulation; thermal simulation; validation

Citation: Korres, D.N.; Papingiotis, T.; Koronaki, I.; Tzivanidis, C. Thermal and Optical Analyses of a Hybrid Solar Photovoltaic/Thermal (PV/T) Collector with Asymmetric Reflector: Numerical Modeling and Validation with Experimental Results. *Sustainability* **2023**, *15*, 9932. https://doi.org/10.3390/su15139932

Academic Editor: Cristina Ventura

Received: 10 April 2023
Revised: 6 June 2023
Accepted: 15 June 2023
Published: 21 June 2023

1. Introduction

Renewable energy resources, such as solar energy, are considered an effective means to address the energy crisis, due to fossil fuel depletion, increased energy demand, and the environmental impact of CO_2 emissions. Solar energy can be utilized for a wide range of applications, from domestic hot water and domestic heating and cooling to industrial applications and electricity production by ensuring lower conventional sources consumption and more useful energy production which leads to sustainability. The simplest way to exploit solar energy potential is by employing solar collectors, which can transform solar energy into heat, electricity, or both.

There are multiple types of solar collectors manufactured [1] based on the required applications, namely flat plate collectors (FPC), evacuated tube collectors (ETC), parabolic

trough collectors (PTC), compound parabolic collectors (CPC), Fresnel lens collectors (FLC), PV/T Collectors, and others.

FPC have been examined by many researchers. Kalogirou [2] investigated possible configurations in order to optimize the system performance through modelling and simulation. The slope of the collector, several riser and tube diameters as well as distances between the top of the collector to the bottom side of the storage tank were analyzed. Korres and Tzivanidis [3] performed a computational fluid dynamic (CFD) analysis on a flat plate collector with a serpentine flow system and examined the effect of the inclination angle and the effect of the natural convection in the air. Subiantoro and Ooi [4] developed analytical methods for the calculation of the heat losses from the top of the collector. Wang et al. [5] performed a comparative analysis of the convection and radiation heat losses on the surface of FPC for different altitudes and studied the effects of the environmental conditions such as air pressure and density. He et al. [6] conducted an experimental analysis on the effect of nanofluids on flat plate collectors' efficiencies and calculated the optimum concentration of nanofluids.

The performance of parabolic trough collectors has been studied extensively, both experimentally and analytically, by numerous researchers. Valenzuela et al. [7] presented a method for the experimental analysis of parabolic trough collectors, in order to determine the thermal and optical performance. Tzivanidis et al. [8] conducted a thermal and optical analysis of a parabolic trough collector under several operating conditions using both numerical and CFD analysis. Zou et al. [9] applied Monte Carlo ray-tracing methods to investigate the effect of the sun shape and incident angle on the optical performance of the collector. Shajan and Baiju [10] used a secondary reflector to homogenize the heat distribution on the receiver. Xu et al. [11] evaluated the performance of parabolic trough collectors under transient conditions and validated the results with experimental data.

Compound parabolic collectors have also been investigated through numerical methods, simulating processes or experimentally. Su et al. [12] performed a theoretical ray-tracing analysis on the compound parabolic collector. Santos-Gonzalez et al. [13] developed a one-dimensional numerical model for the thermal performance of the collector, which was then validated by experimental results. Tchinda [14] examined the heat transfer within a CPC with a flat one-sided absorber, while Antonelli et al. [15] proposed a two-dimensional CFD methodology for the estimation of thermal losses for both a circular and flat receiver. Korres et al. [16] studied the thermal performance of both pure thermal oil and thermal oil with nanofluids with computational simulations. Finally, Korres and Tzivanidis [17] investigated experimentally and numerically the operation of an asymmetric compound parabolic collector.

Regarding the evacuated tube collectors, Korres et al. [18] carried out an experimental and numerical analysis of a U-type evacuated tube collector array with mini compound parabolic concentrators in order to calculate the thermal efficiency of the system. Nitsas and Koronaki [19] developed a mathematical model for the energy and exergy efficiency of an evacuated tube collector, which was validated by experimental data. Ismail et al. [20] performed a comparative study of a evacuated collector with a circular and a rectangular absorber with heat transfer fluids enhanced with nanofluids.

Concentrating technologies were implemented not only in solar thermal systems but also to photovoltaic cells. For PV applications, concentrating systems were found to achieve higher flux intensity and as a result higher electricity production than the cells without concentrators. Li et al. [21] analyzed numerically and experimentally a novel asymmetric compound parabolic concentrator which can achieve uniform flux distribution on the PV cell. Renzi et al. [22] conducted an experimental analysis of a commercial CPV system under real outdoor operating conditions. Sangani and Solanki [23] examined the gain in output power by using a 2-sun V-trough concentrator with a commercially available PV module.

More recently, PV/T systems have been proposed. In PV/T collectors, PV modules are combined with heat recovery units in order to simultaneously provide heat and electricity

from the same aperture area, [24] therefore fulfilling both thermal and electricity needs either for domestic [25] or larger scale applications [26], while at the same time increasing the efficiency of the PV module by reducing its temperature. There are two main types of hybrid solar collectors: flat plate and concentrating.

Numerous studies have been undertaken which examined PV/T collectors both numerically and experimentally. Regarding the flat plate hybrid solar collectors, Jonas et al. [27] simulated the performance of both a covered and uncovered collector and validated the results by experimental data. Lämmle et al. [28] built two novel PV/T collectors with overheating protection and tested the effect of this protection on the temperature of the absorber and the efficiency of the system. Lämmle et al. [29] studied the effect of low-emissivity coatings on heat losses and electrical production, by numerical models and experimental studies and compared the results with a collector with the same design but without the coating. Herrando et al. [30] modelled numerous alternative absorber-exchanger designs through a three-dimensional computational finite element method and performed a comparative techno-economic analysis of the proposed designs with a reference commercially available PV/T collector. Finally, Guarracino et al. [31] conducted a coupled thermal and electrical analysis of a sheet and tube hybrid photovoltaic/thermal collector under dynamic conditions by developing a 3D numerical method.

The use of concentrating collectors has been found to lower the number of PV cells, thermal absorber materials, and heat losses and raise the operating temperatures [32]. Koronaki and Nitsas [33] investigated experimentally the performance of five asymmetric hybrid solar collectors connected in series and developed a mathematical model based on the experimental data to evaluate the performance of the system under different operating conditions. Proell et al. [34] constructed and carried out an experimental analysis on a stationary flat plate concentrating CPC PV/T solar collector. In this study, the angle dependent electrical and thermal performance of the collector was measured. Nilsson et al. [35] performed a long term evaluation of an asymmetric compound parabolic reflector system with two truncated parabolic reflectors. This system was designed for high altitudes and data for the estimation of the annual thermal and electrical output were presented. Nasseriyan et al. [32] conducted a 2D CFD analysis of an asymmetric CPC collector which was validated by experimental results. The effect of different parameters on the thermal and the electrical production were studied.

Most CFD analyses model the effect of the air or the inert gas between the glass cover and the reflector, in the case of concentrating collectors, or between the glass cover and the absorber, in the case of FPC, by developing the necessary mesh grid. For example, at Refs. [15,32] the air was modeled while performing a 2D analysis. The same methodology was used at 3D analysis at Ref. [30] for a flat plate PV/T collector and at Ref. [36] for a CPC.

However, modeling the air at the interior of a gap requires significantly high computational resources being conducted, considering that in most cases a great percentage of the mesh elements corresponds to such regions. This is very inconvenient in cases in which the main goal is to calculate the thermal performance, and the air gap function is of low relevance. Hence, the need arises for an alternative method to fill this research gap effectively and efficiently. To this end, in the present study, a novel numerical method was developed which enables the calculation of the collector's thermal performance without modeling the air function inside the gap. Thus, the proposed method offers a very promising sustainable solution, since its implementation could save valuable computational time and resources.

This study presents a combined thermal and optical, three-dimensional analysis of an asymmetric compound parabolic collector (ACPC) with an integrated hybrid photovoltaic/thermal (PV/T) receiver. Initially, the authors calculated the Incident Angle Modifier (IAM) for a wide range of incident angles and the ray-tracing results were verified using three different simulation tools (Tonatiuh, COMSOL, and SolidWorks). The optimal tilt angle of the collector was determined for seven months of the year by conducting a detailed ray-tracing analysis for the mean day of each month considering whole

day operation. The specific optimization process was followed to take advantage of the maximum possible solar irradiation in each month and, thus, to ensure the highest possible optical performances with the same geometry, which significantly enhances the sustainability of the proposed system. In the thermal analysis part, a novel numerical modeling method was developed and proposed by the authors for the numerical simulations. This method was then established via two different simulation tools: COMSOL and SolidWorks. The numerical models which were built in the aforementioned programs were verified with each other and validated through experimental results taken from the literature regarding the examined collector. Finally, the thermal performance of the collector was investigated for the mean day of September at solar noon by adopting the optimal tilt angle for that month according to the optical analysis, considering inlet temperatures from 20 °C up to 80 °C.

In conclusion, the innovative simulation method presented in this study could offer notable benefits; firstly, it can be applied to numerous similar geometries. In addition, in terms of feasibility, it allows for the calculation of the optimum tilt angles of the collector for seven months of the year, thus serving as a guide for installation and exploitation of solar energy. This presents an added advantage in the case of this specific collector considering its commercial availability and applications. Finally, it should be mentioned that the modeling method developed requires less computational time than the conventional CFD methods to generate the desirable results, thus adhering to the fundamental principles of sustainability.

2. Materials and Method

2.1. The Solar Collector

An ACPC with PV/T absorber is investigated in this work. The examined collector consists of an asymmetric reflector formed by the combination of a parabolic and a circular profile. The focal point of the parabolic part is located in the center of the circular one, while the focal distance is perpendicular to the aperture width. The PV/T receiver has three layers on each side (silicone–PV–silicone) which adhere to the main aluminum substrate consisting of eight elliptic fluid conduits for the heat transfer fluid. Each PV consists of two strings of 38 mono-crystalline type cells with nominal efficiency of 18.7% and a cell temperature coefficient of 0.4%/°C. The silicone layers were applied on both sides in order to effectively conduct the heat from solar cells and protect the cell from moisture, UV radiation, and simultaneously provide electrical insulation [33]. Figure 1 illustrates the geometry of the collector and the details of the receiver layers.

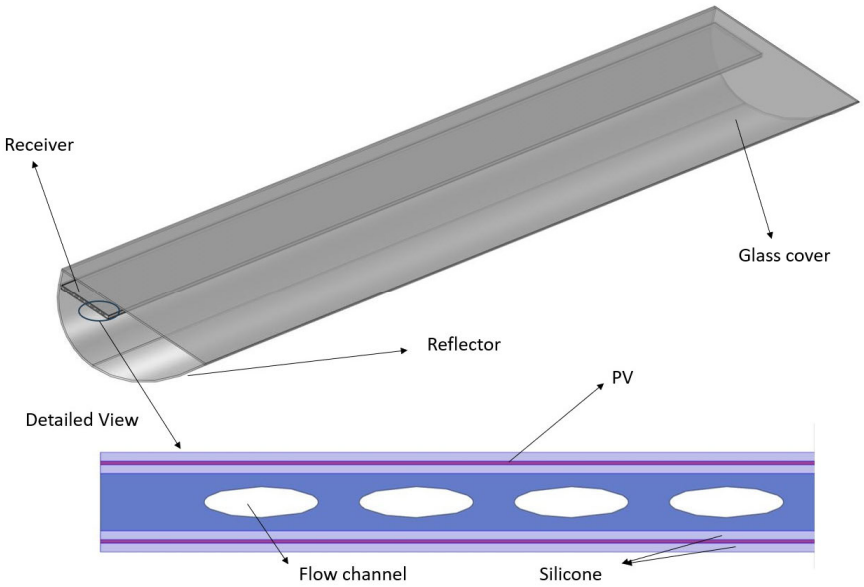

Figure 1. Three–dimensional (3D) collector's geometry and detailed view of the receiver.

Specifically, the useful length of the collector is 2.29 m with a width of 0.464 m. The focal length of the collector parabola is 144.86 mm. The radius of the circular profile is equal to the focal distance. The reflector is 4 mm thick, with an emissivity of 0.05 and reflectivity of 94%. The receiver is made of aluminum and the main dimensions are: 2.29 m length, 0.158 m width, and a thickness of 6.5 mm. It consists of 8 elliptic channels, each having a semi major axis and a semi minor axis of 7 mm and 1.75 mm, respectively. The receiver has two rows of PV panels, on the front and at the back, which are identical. The collector is protected by glass with solar transmittance of 95%. The optical characteristics of the collector are available in Table 1 [32].

Table 1. Optical characteristics of the collector [32].

Parameters	Values
Cover emittance	0.95
Cover transmittance	0.95
Reflector emittance	0.05
Reflector reflectance	0.94
Receiver absorptance	0.93
Receiver emittance	0.90

The main geometrical characteristics of the collector are summarized at Table 2 and a 2D schematic depiction with the main dimensions of the collector is available in Figure 2.

Table 2. Geometrical characteristics of the collector [32].

Parameter	Value
Collector Length	2.29 m
Collector Width	0.464 m
Receiver Width	0.157 m
Geometrical Concentration ratio	1.51
Reflector Parabolic Profile Focal Length	0.144 m
Reflector Circular Profile Radius	0.144 m

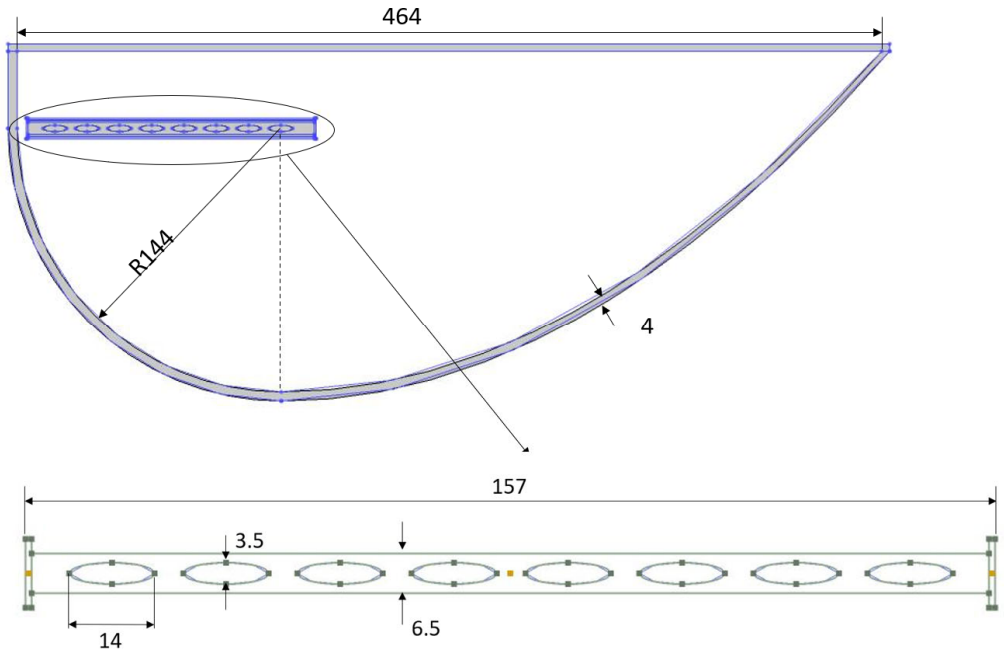

Figure 2. Main dimensions of the solar collector.

2.2. Mathematical Modeling

In this subsection, the mathematical equations used for the thermal and optical analysis are given. First of all, the Incidence Angle Modifier (IAM) is calculated using Equation (1) [37].

$$IAM(\theta) = \frac{Q_{abs}(\theta)}{Q_{abs,max}} \quad (1)$$

where Q_{abs} is the total power absorbed by the receiver, from both the top and the bottom surfaces, as calculated during ray tracing for each incident angle and $Q_{abs,max}$ expresses the maximum possible absorbed solar power.

The optical efficiency was selected to be calculated by Equation (2) [17], to take into consideration the effect of the incident angle change.

$$n_{opt} = \frac{Q_{abs}}{Q_{s,max}} \quad (2)$$

Parameter $Q_{s,max}$ corresponds to the maximum possible solar power, which could be available on the aperture of the collector and which is equal to the product of the effective solar irradiation in a plane perpendicular to the solar rays with the aperture area of the collector as Equation (3) [17] shows.

$$Q_{s,max} = A_c \cdot G_{eff,n} \quad (3)$$

Regarding the $G_{eff,n}$ parameter, it expresses the effective solar radiation that falls to a plane perpendicular to the solar rays, and it is expressed via Equation (4) [17].

$$G_{eff,n} = G_{b,n} + \frac{G_d}{C} \quad (4)$$

The G_d parameter is the diffuse solar radiation intensity while parameter C is the concentration ratio which is the quotient between the aperture area and the surface area of the receiver, as shown in Equation (5) [17].

$$C = \frac{A_c}{A_r} \quad (5)$$

The thermal efficiency of the photovoltaic-thermal collector is defined by Equation (6) [38].

$$\eta_{th} = \frac{Q_u}{A_r \cdot G_{eff,T}} \quad (6)$$

Regarding the $G_{eff,T}$ parameter, it expresses the effective solar radiation that falls perpendicular on the collector's aperture, and it is given via Equation (7) [17].

$$G_{eff,T} = G_{b,T} + \frac{G_d}{C} \quad (7)$$

The Q_u parameter is the useful heat, which is calculated by Equation (8) [17,33].

$$Q_u = m_f \cdot C_{p_f} \cdot \left(T_{fo} - T_{fi}\right) \quad (8)$$

Parameter m_f expresses the mass flow rate of the working medium and it is being produced with the specific heat capacity of the medium (C_{p_f}) and the inlet to outlet temperature difference ($T_{fo} - T_{fi}$), in order to give the useful power.

The temperature of the sky (T_{sky}) used for the calculation of the radiative heat losses of the glass cover and the reflector to the ambient, is determined by the Equation (9) [18].

$$T_{sky} = 0.0552 \cdot T_a^{1.5} \quad (9)$$

The convective heat-transfer coefficient between the outside surfaces of the collector and the ambient air is calculated by Equation (10) [32].

$$h_{out} = \frac{8.6 \cdot u^{0.6}}{L^{0.4}} \tag{10}$$

Parameter u (m/s) is the speed of the wind and L (m) is the length of the collector.

The temperature of the PV cells affects their electric efficiency, which can be described by Equation (11) [33].

$$\eta_{el} = \eta_{ref} \cdot \left(1 - \beta_c \cdot \left(\overline{T_{pv}} - T_{ref}\right)\right) \tag{11}$$

Parameter η_{ref} is the efficiency of the cell under standard test conditions (STC, $G = 1000 \frac{W}{m^2}$, $T_{ref} = 25\ ^\circ C$) and β_c is the temperature coefficient of the PV [32,33].

Considering average temperature for the PV on each side of the receiver, the electrical production is calculated by Equations (12)–(14) [32,33]:

$$P_{el,top} = G_T \cdot A_r \cdot \eta_{ref} \cdot \left(1 - \beta_c \cdot \left(\overline{T_{pv,top}} - T_{ref}\right)\right) \tag{12}$$

$$P_{el,bot} = G_{cpc} \cdot C \cdot A_r \cdot \eta_{ref} \cdot \left(1 - \beta_c \cdot \left(\overline{T_{pv,bot}} - T_{ref}\right)\right) \tag{13}$$

$$P_{el,tot} = P_{el,bot} + P_{el,top} \tag{14}$$

where G_{cpc} is defined through Equation (15) [33].

$$G_{cpc} = G_T - \frac{1}{C} \cdot G_d \tag{15}$$

2.3. Numerical Modeling

2.3.1. Simulation Tools

In the present work, three different simulation software were used for the evaluation of the collector's optical and thermal operation. In particular, Tonatiuh software (release 2.2.4) was used for the ray-tracing analysis and it was verified by the ray-tracing environments of COMSOL and SolidWorks programs. The last two software were used for the thermal analysis simulations and their results were validated by experimental data from the literature study [32] in which the collector of the present analysis is examined.

Tonatiuh is an open-source ray-tracing software developed by the National Renewable Energy Center (CENER), which uses Monte Carlo methods for the simulation of concentrating solar systems [39]. Through a Graphical User Interface, the software allows the user to design complex geometries by combining a wide range of shapes, and to define the optical parameters of the surfaces of the collector by modifying the available material groups. The results obtained by the program have been validated with experimental data from different systems and the software has been used in numerous research studies in the field of the performance analysis of solar thermal collectors [37,40].

COMSOL is a commercial software which utilizes the finite element's methods to solve multi-coupled physics problems [41]. In order to setup the simulation procedure it is essential to define the materials on each volume and surface, construct the examined geometry, specify the appropriate physics modules and the necessary boundary conditions, mesh the model and finally select and setup the solver. COMSOL is a widely used software in research work for flat plate [42,43] and concentrating solar collectors [44].

SolidWorks [45] is a widely used simulation package which has been applied in numerous studies regarding energy systems and especially in solar thermal collectors' applications [3,8,16,46,47]. The program supports design and it is suitable for a wide range of applications by ensuring flow, optical, and thermal simulations are conducted either separately or simultaneously, while it has been validated with experimental results in

numerous studies [17,18,48]. The flow simulation environment is the interface in which the numerical modeling takes place.

2.3.2. Ray-Tracing Analysis

This section presents the ray-tracing analysis in detail. Initially, the geometry of the collector is developed in each program used (COMSOL, SolidWorks, and Tonatiuh). After the shape of the collector has been created, the optical behavior of the system is investigated considering the modification of the incident angle in the transversal direction and at a variety of incident angles of solar irradiance. By varying the direction of solar rays, the IAM is calculated by using Equation (1).

For the calculation of this index, solar direct irradiation was kept constant at 1000 W/m^2. It is important to mention that the sunshape is simulated as pillbox in each of the three packages. The input data for the ray-tracing analysis are given in Table 3.

Table 3. Parameters of the ray-tracing analysis.

Parameter	Value
Intensity of Solar irradiance	1000 W/m^2
Solar rays	10^6
Incident angle (transversal direction)	0–60°

After the results of the optical analysis were verified among the utilized simulation tools, Tonatiuh software was selected and the optimal tilt angle of the collector was determined for the period from March to September at the mean day of each month in Athens, Greece. The optical efficiency of the collector was calculated for a total duration of 10 h, from 7:00 to 17:00, and for a range of tilt angle from 0° to 40°, for each examined day. The aim was to calculate the most suitable inclination angle in each case so as to utilize the maximum possible solar irradiation, which is an essential factor for ensuring the sustainability of the system.

For the simulation, the collector was southwards oriented and the latitude and longitude for the area of Athens were set to 37.98° and 23.93°, respectively. Finally, the position of the sun and the resulting direction of the incoming direct irradiation was calculated by Tonatiuh based on the time, date, and coordinates given as an input according to the libraries of the program.

After the optical simulations, the optimum inclination angle was calculated for each mean day examined.

2.3.3. Thermal Analysis Modeling Method

The thermal analysis of the examined configuration was conducted via simulation with SolidWorks and COMSOL, as regard to the experimental validation process. After the validation of both programs with experimental results, COMSOL Multiphysics software was applied for the main thermal analysis.

The method applied for the thermal simulations was developed by the authors of the present study and is novel as it considers the air enclosed between the glass and the reflector, without including it in the numerical modeling, thus saving valuable computational time. Consequently, the developed method offers a highly sustainable solution in numerical modeling, since fewer physical resources are being spent in order to obtain the desirable results. In other words, the enclosed air was not included in the computational domain and, therefore, it was not solved by the simulation tools. In particular, the enclosed air presence was achieved by applying boundary conditions regarding its temperature and the corresponding convective heat-transfer coefficient on all the receiver surfaces, on the inner sides of the glass and on the inner sides of the reflector. In each simulation, this convective heat-transfer coefficient was assumed to be constant while several different values for the enclosed air temperature were tested until the overall thermal losses coming from the receiver were equal with these produced from the outer surfaces of the collector.

This was the main criterion for convergence of the solution at each operating point, since these two losses must take the same values for the energy balance of the collector to be fulfilled. To properly calculate the overall heat losses, both the radiative and the convective contribution were considered.

Initially, a random temperature value for the enclosed air was applied to all the air gap surfaces to calculate the convective heat losses. This temperature value is taken between the inlet water temperature and the outer air temperature. After the numerical solution is completed, the overall heat losses coming from the receiver and the corresponding heat loss from the outer surfaces of the collector are determined. A higher value in the gap air temperature is given in case the receiver thermal losses are higher than the respective losses from the outer surfaces. More specifically, by providing a higher temperature value for the gap air, then the receiver overall losses are going to decline while the outer surfaces will have a higher temperature and the overall losses coming from them will increase. Hence, this procedure is repeated until the overall thermal losses are balanced. The procedure was conducted for some of the tested operating points, and it was revealed that it gives approximately the same results with the linear interpolation between two test points with 1 K difference in the assumed enclosed air temperature (T_{ai}). Table 4 gives an example of how the modeling method was applied in terms of solution convergence.

Table 4. Solution convergence example.

Test Point	T_{ai}	$T_{f,i}$	$T_{f,o}$	$Q_{losses,1}$ (from Receiver)		$Q_{losses,2}$ (from Outer Surfaces)
1	23	36.2	38.65	134.9	>	123.7
2	24	36.2	38.68	130.7	<	133.5
Linear interpolation	***23.8***	***36.2***	***38.674***	***131.54***	**=**	***131.54***

In this way, it was possible to study the overall operation of the examined collector without simulating the air function at the interior of the gap between the reflector and the glass plate, which introduces a novel characteristic of the developed method, ensuring significant computational time and cost saving.

Regarding the type of the solution followed, steady-state analysis was conducted both in the experimental validation and in the main thermal analysis. Throughout the analysis, laminar flow was assumed as the governing flow regime in accordance with reference [32], in which the same volumetric flow rate was applied. In the experimental validation, the steady state solution was followed in order to adhere to the experimental method applied in study [32]. While in the main thermal analysis, the solution was deliberately conducted in steady-state conditions, so as to study only the effect of the inlet temperature increment on the thermal efficiency. On the other hand, the optical efficiency investigation was conducted considering time-dependent analysis type, to examine the incident angle effect on the optical performance of the collector.

2.3.4. Mesh Independency

A mesh independency procedure was conducted in the present work. This procedure was put forward regarding the models developed both in COMSOL and in SolidWorks environment in order to obtain results which are independent of the grid size. The mesh independency procedure was focused on the thermal efficiency convergence. In particular, the mesh elements on the interfaces between the water and the conduits' walls were refined, while the fluid domain mesh was, also, examined and refined properly to ensure proper heat-transfer modeling between the water and the walls. The grid on all the absorbing and reflecting surfaces was refined to avoid misfunctions with solar absorption and to achieve sufficient ray tracing.

The mesh independency procedure of the model developed in COMSOL is presented below, since this model was used mainly in this study. Three different meshes were tested regarding the first experimental point, according to Section 2.4, with the main criterion

being the convergence of the thermal efficiency of the collector. The meshes that were applied in the developed model are given in Table 5. While the results of the independency procedure are plotted on Figure 3.

Table 5. Mesh independency of the numerical model in COMSOL.

Mesh Name	Mesh_1	Mesh_2	Mesh_3
Total Mesh Grid Elements ($\times 10^6$)	0.60	0.75	0.95
Water Mesh Grid Elements ($\times 10^6$)	0.16	0.28	0.48
Receiver Mesh Grid Elements ($\times 10^6$)	0.26	0.27	0.33

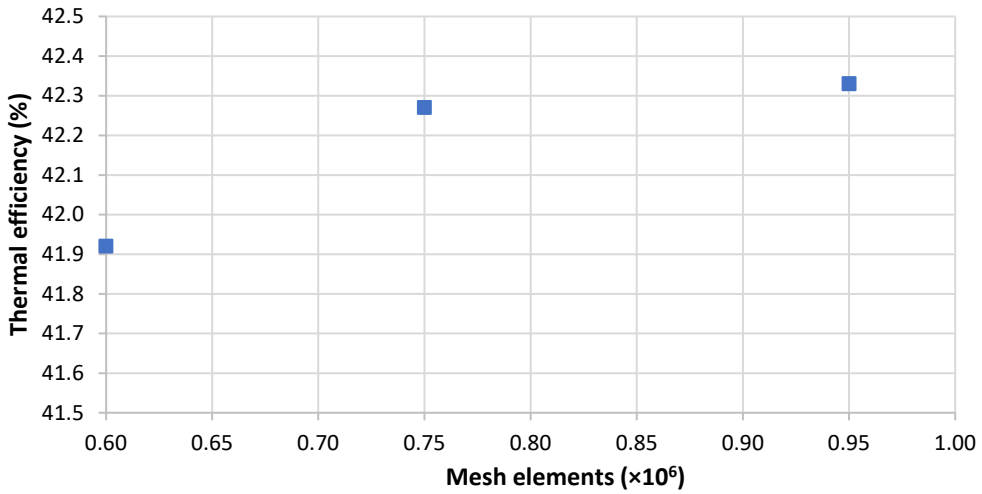

Figure 3. Mesh independency of the numerical model in COMSOL.

The mesh independency results indicated that the increment of the mesh elements result in the convergence of the thermal efficiency values. Hence, the third mesh was applied for the numerical simulations. Figure 4 shows the mesh grid structure on the examined collector in the fluid region and in the components of the collector.

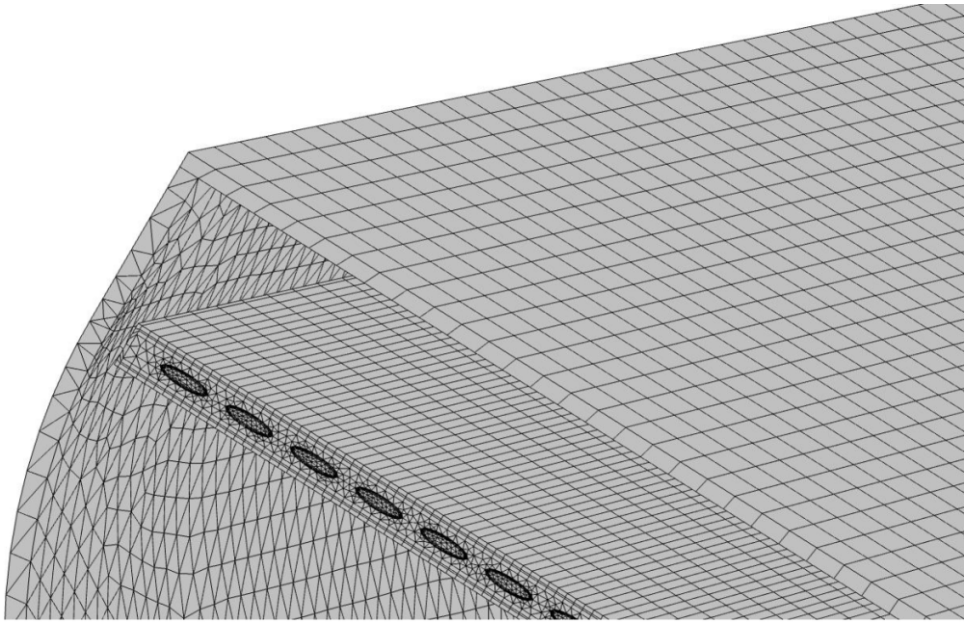

Figure 4. Mesh structure of the model in COMSOL.

2.3.5. Operating Conditions in Thermal Simulations

The main thermal analysis of the collector was conducted for solar noon of the mean day of September, considering the optimum slope of the collector for the particular time and day which takes the value of 30°. The hybrid collector was examined for inlet temperatures of 20 °C up to 80 °C with a 2.2 lt/min volumetric water flow rate, which are reasonable values for the particular application [32]. The Photovoltaic Geographical Information System (PVGIS) [49] was used for values regarding solar irradiance while the ambient temperature and the wind velocity for the mean day of September were taken from the Technical Notes of the Technical Chamber of Greece [50]. The direct beam solar irradiation in a plane normal to solar rays was 653 W/m^2 and the diffusive portion of solar irradiation took the value of 230 W/m^2. The environmental air temperature was set to 25.5 °C and the wind velocity was equal to 3.6 m/s. From Equation (10) the heat-transfer coefficient of the wind was calculated and took the value of 13.3 $W/m^2/K$. As mentioned in Section 2.3.3, the convective heat-transfer coefficient of the enclosed air gap was assumed to be constant and equal to 5 $W/m^2/K$, which is a reasonable value for such closed areas while similar values could be found in studies [3,36]. The thermal simulation operating conditions are, also, available in Table 6.

Table 6. Thermal simulation boundary conditions.

Parameter	Value	Units
Direct Solar Irradiance	653	W/m^2
Diffusive Solar Irradiance	230	W/m^2
Sun Rays	10^6	rays
Environment Air Temperature	25.5	°C
Wind Velocity	3.6	m/s
Wind Heat Transfer Coefficient	13.3	$W/m^2/K$
Enclosed Air Heat Transfer Coefficient	5	$W/m^2/K$
Inlet Water Temperature	20–80	°C
Volumetric Water Flow rate	2.2	lt/min

It must be mentioned that the boundary conditions presented in Table 6 were set properly for the entire collector geometry. In particular, the environment temperature and the wind heat transfer coefficient were both set on all the outer surfaces of the collector. The heat-transfer coefficient inside the air gap was defined on all the inner collector surfaces which come into contact with the enclosed air. The inlet water temperature values were set at the inlet of the collector while the volumetric flow rate was set at its outlet.

2.4. Experimental Validation

It was essential to validate the function of the two simulation software used, COMSOL and SolidWorks. For this reason, experimental data from Nasseriyan et al. [32] were utilized and the results of the combined thermal, optical, and flow simulation conducted in COMSOL and SolidWorks were validated. Study [32] was selected, since the same collector is examined with water as the working fluid. The experimental data are given in Table 7.

Table 7. Experimental data [32].

Experimental Point	G_{bT} (W/m^2)	G_d (W/m^2)	Ta (°C)	$T_{f,i}$ (°C)	$T_{f,o}$ (°C)	V_f (lt/min)
1	978.3	93.1	18.6	33.6	36.6	2.2
2	757.8	145.5	21.6	36.2	39	2.1
3	946	77.2	20.1	46.3	48.4	2.2

The mean wind velocity was considered to be 3.14 m/s during the measurements [32], which corresponds to a convective heat-transfer coefficient of 12.22 $W/m^2/K$, according to Equation (10). The experimental values of the effective solar irradiation intensity, which

were calculated by Equation (4), the environment air temperature, the inlet water temperature, the volumetric water flow rate, and the convective heat-transfer coefficient of the wind were set as inputs in the simulations.

3. Results and Discussion

3.1. Ray Tracing Simulation Verification

An initial step, before proceeding with the main analysis of the collector, was the verification of the ray-tracing simulation results. The ray-tracing simulations were conducted via three different programs: Tonatiuh, COMSOL, and SolidWorks. The data for the simulation were taken from Table 3. Figure 5 gives the comparison among the three developed ray-tracing simulations as regard to the Incident Angle Modifier (IAM) of the collector.

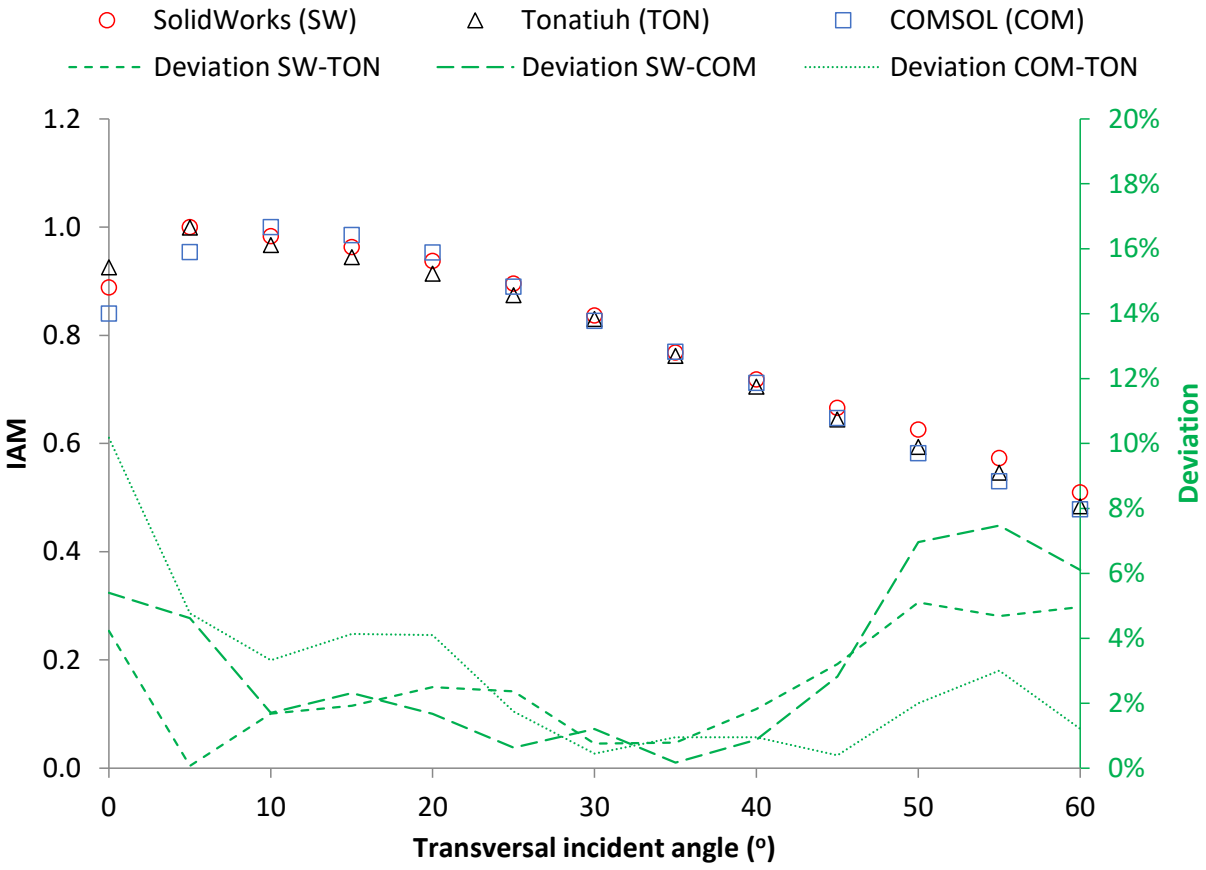

Figure 5. Ray-tracing results verification.

As seen in Figure 5, the IAM increases for values of the incident angle between 0 and 5° and reaches its maximum value at 5°. For higher incidence angles the IAM decreases. This result is expected because of the specific asymmetric geometry of the reflector. In addition, from Figure 5, it becomes obvious that there is sufficient agreement between the three models with the mean deviations lower than 4%. In particular, the three ray-tracing models seem to follow the same trend and to ensure low deviations among them for a wide range of transversal incident angles. The mean deviation between the ray-tracing models developed in Tonatiuh and in COMSOL hardly reaches 3%, while the respective deviation in the comparison between Tonatiuh and SolidWorks takes the value of 2.6%. Hence, the three simulation tools seem to provide reliable and valid results as regard to ray tracing. For this reason, Tonatiuh software was selected for the main optical analysis part in Section 3.2. Figure 6 illustrates the ray-tracing visualization in Tonatiuh software (release 2.2.4) for the examined configuration.

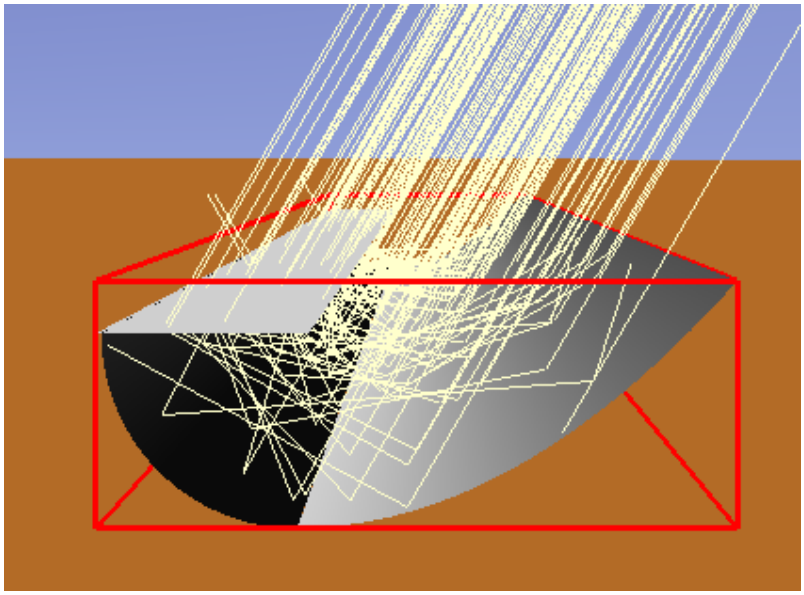

Figure 6. Ray-tracing modeling of the collector in Tonatiuh.

3.2. Results of the Validation with Experimental Data

The validity of the numerical models was evaluated with experimental results taken from study [32]. To this end, three experimental points were utilized, and compared in terms of thermal efficiency. The numerical models were, also, verified between each other as far as their usefulness and the electrical output are concerned. The results of the particular comparisons are depicted in Figure 7.

As observed in Figure 7a, the numerical results appear to be very close to the respective experimental results with maximum deviations lower than 10%. More particularly, each one of the numerical models exhibited mean declination from the experimental results of less than 6%. Moreover, the numerical models are in close agreement with each other, since the maximum deviation between them is equal to 6.15%. Close agreement between the numerical models is also obvious in Figure 7b in which the electrical and the useful power are presented. In that depiction, it seems that apart from the fact that the values are close to each other, the trend of the results appears to be similar in the two models. According to the prementioned comments, the proposed method seems to be valid and to provide reliable results by sufficiently simulating the real operating conditions.

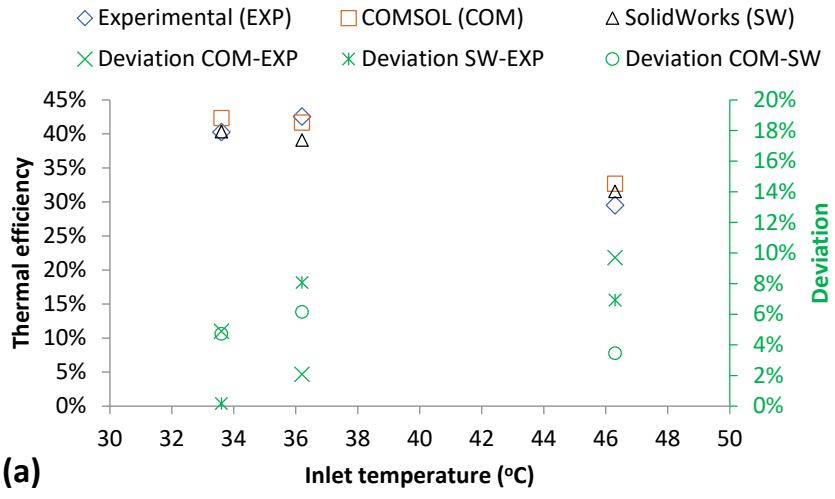

Figure 7. *Cont.*

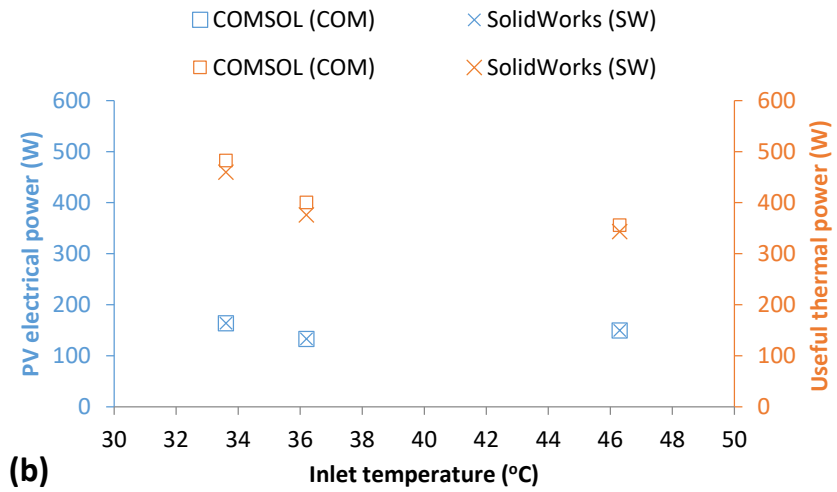

Figure 7. (**a**) Experimental validation and (**b**) Numerical models verification.

3.3. Optical Performance Analysis

The optical performance analysis results are available in the present section. As is stated in Section 2.3.2, the collector optical performance was examined for seven months of the year in Athens, Greece, for the mean day of each month, considering the data which are available in Section 2.3.2. The inclination angle was modified in each case to determine the optimum one for each hour of the day. Indicative detailed results of three of the examined months are given in Figure 8 to avoid confusion in the results evaluation.

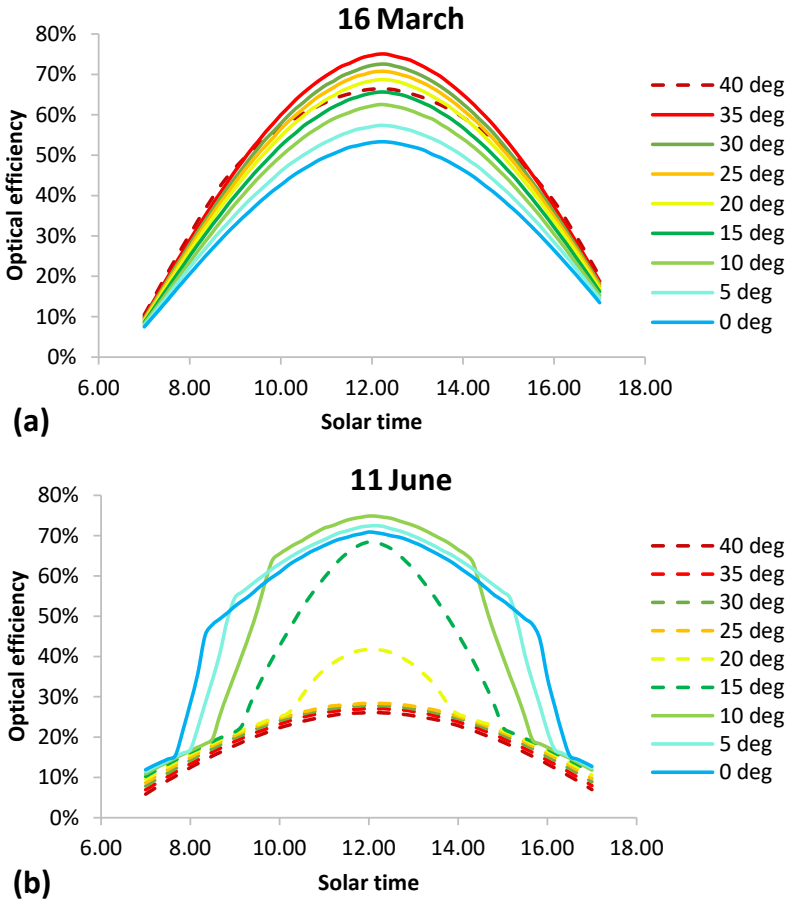

Figure 8. *Cont.*

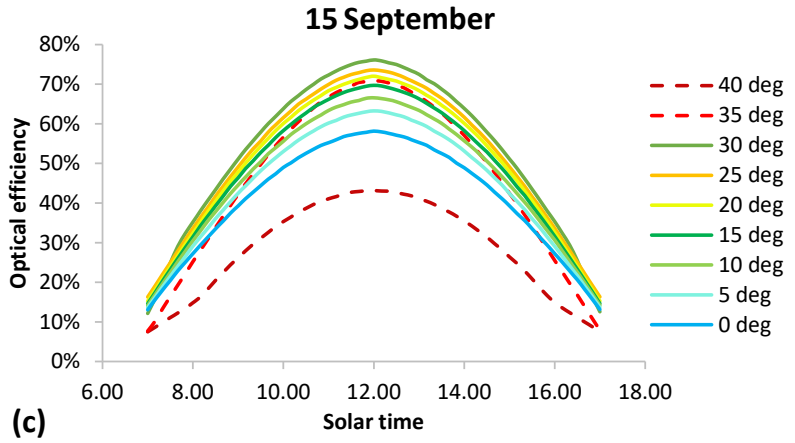

Figure 8. Daily optical efficiency results: (**a**) 16 March, (**b**) 11 June, and (**c**) 15 September.

From Figure 8, it could be seen that the optical efficiency is dependent on the inclination angle of the collector in all cases. High optical efficiency values of up to 76% appear in all months around solar noon. It is, also, worth noting that abrupt changes and a sharp decrease in optical performance (see Figure 8b) occur mostly early in the morning and late in the afternoon when the inclination angle increases. This is due to the fact that when the collector is tilted, the transversal incident angle lowers significantly or it becomes negative, especially in early morning or late afternoon hours, which means that the sun, in those cases, is behind the collector. Thus, the reflector does not participate in solar utilization and, as a consequence, the aperture of the collector in those cases decreases abruptly and dramatically.

Moreover, the optimum slope varies from hour to hour and from month to month due to changes in the sun's position. On a monthly basis, this difference occurs due to the change of the solar declination "δ" [51], which is equal to zero on 21 June. According to Figure 8, from 16 March to 11 June, the optimum inclination angle decreases since the sun rises higher in the sky, while after 21 June the slope increases since the sun moves lower. This could be observed in more detail via Figure 9, in which the optimum tilt values are plotted for each operating hour and each month. The months after June are plotted with dashed lines to better illustrate the effect of the season in the optimum inclination angle. The results depicted are only for the morning hours given that the same results hold for hours after 12:00 solar time. For example, the optimum tilt for 13:00 is equal to the respective optimum tilt for 11:00.

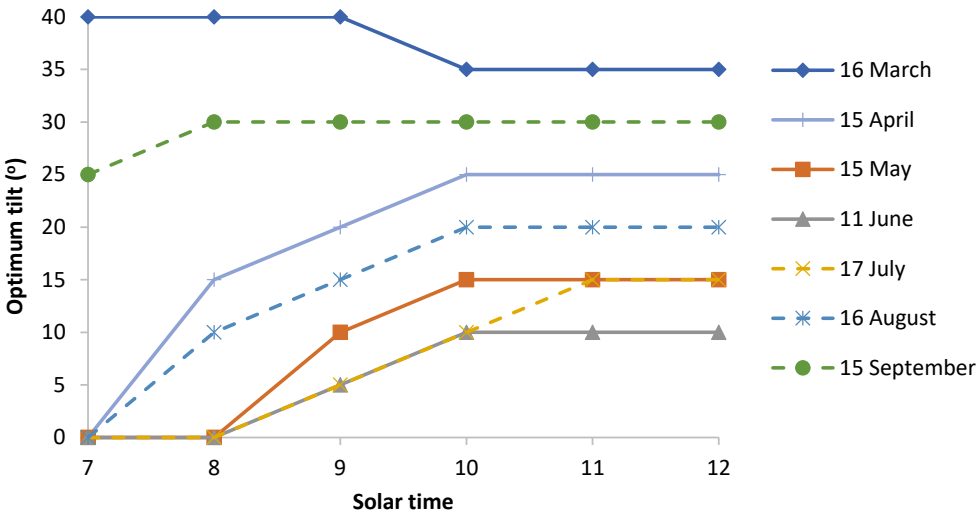

Figure 9. Optimum tilt of the collector for each operating hour of each mean day.

Figure 9 indicates that the optimum tilt of the collector decreases from April to June and increases from June to September, for the reasons mentioned above. In addition, on most of the days examined, the optimum inclination angle remains constant around solar noon and especially from 10:00 to 14:00 solar time. Thus, Figure 9 is very useful and could be used as an installation guide when regulating the tilt of the collector in order to maximize the optical performance around solar noon. For example, based on the data depicted in Figure 9, a tilt angle lower than 10° should be avoided in all seasons. If there is a need for a more detailed analysis regarding the tilt effect on the efficiency, then Figure 9 should be used.

3.4. Thermal Performance Analysis

This section presents the thermal operation of the collector under investigation and the respective results. The thermal performance was evaluated considering input data from Section 2.3.5, according to Table 6 for solar noon of the mean day of September, with the inlet temperature varying from 20 °C up to 80 °C. The tilt of the collector for the particular scenario was set at the respective optimum value of 30° according to Figure 9. Results of the analysis regarding the thermal efficiency are presented in Figure 10.

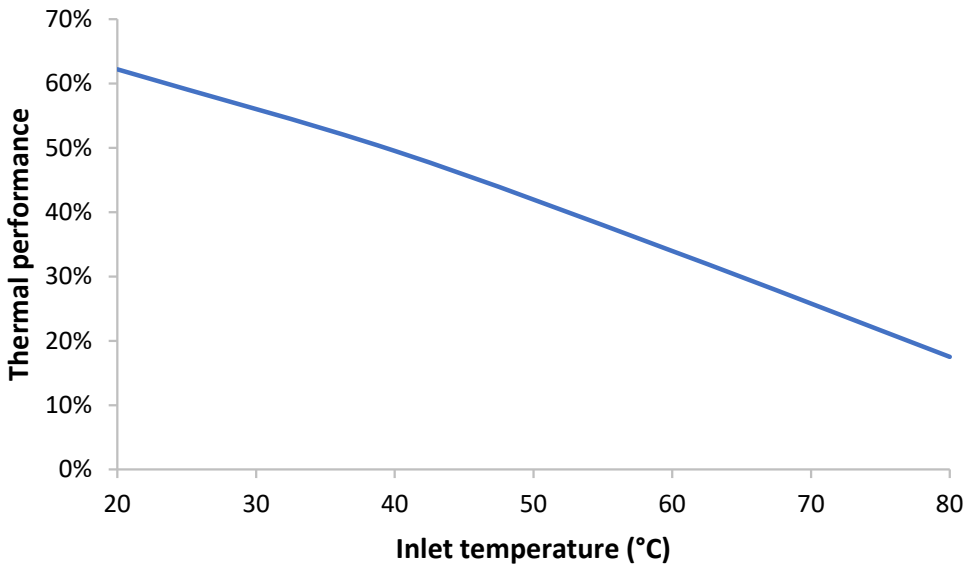

Figure 10. Thermal efficiency of the collector in the entire inlet temperature range.

As observed in Figure 10, the thermal efficiency declines with the increase in the inlet temperature, because the overall heat losses increase. These losses are dependent on the working medium flow rate and thus are inversely related with the useful power of the working medium. In addition, it should also be mentioned that the thermal efficiency reaches 62.2%, which is sufficient considering that the hybrid operation was studied, and thus electrical output is considered additionally. Figure 11 depicts the absorbed solar power, the useful power, the thermal losses, and the electrical output of the collector for the examined inlet temperature range.

As illustrated in Figure 11, the absorbed solar power in each operating point is equal to the sum of the useful power, the electrical power, and the thermal losses so as to reach proper power equilibrium, which indicates that the proposed method provides reasonable results. In more detail, it could be seen that the decrease in the useful power going to higher inlet temperatures is accompanied by increase in the thermal losses, given that the higher the inlet temperature, the higher the temperature level of all the components of the collector and thus the higher the thermal losses. The electrical power gained from the PVs operation appears to decrease with the increment of the inlet temperature and that happens due to

the simultaneous decrease in the electrical efficiency. This reduction happens because of the increment in the PVs temperature.

Figure 12 illustrates the temperature difference between the PVs and the inlet water to investigate differences between the two PV panels and correlate them with the inlet water, in terms of the temperature level.

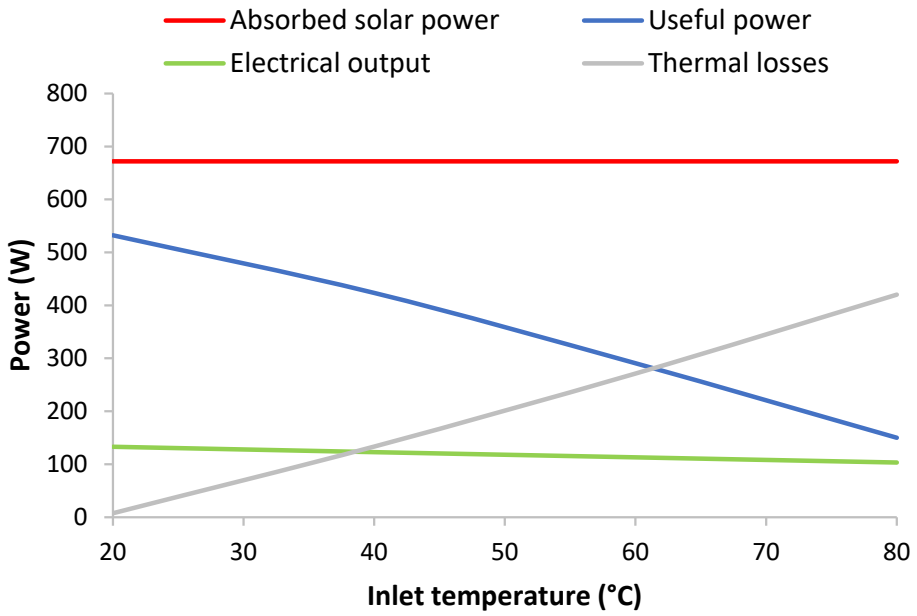

Figure 11. Absorbed solar power, Useful power, Thermal losses, and Electrical output of the collector in the whole inlet temperature range.

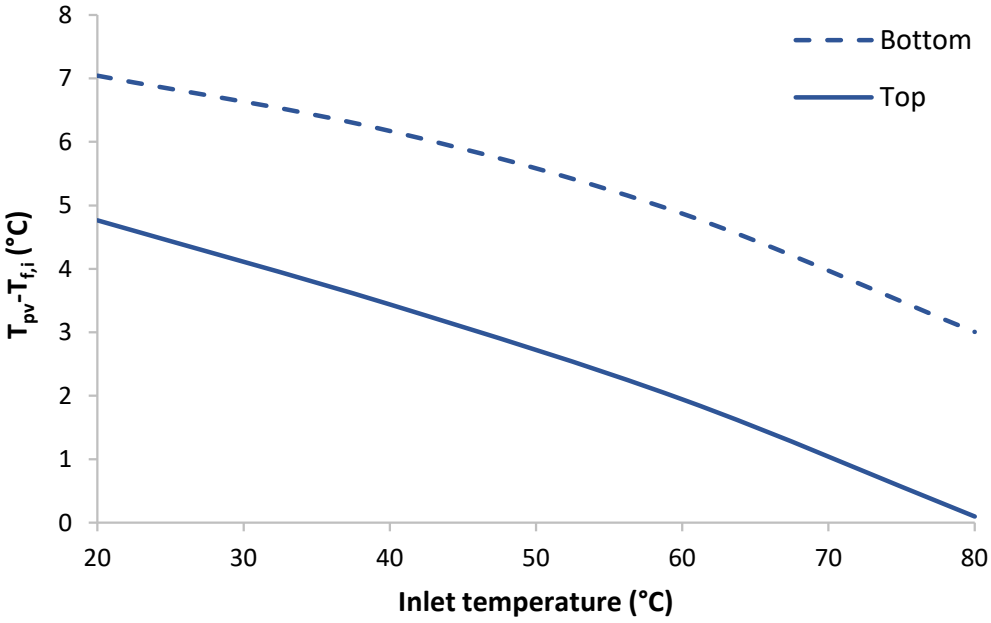

Figure 12. Temperature difference of the bottom and the top PV with the inlet water.

As shown in Figure 12, the PV at the bottom exhibits higher temperatures than the top of the receiver for the entire operating range. This could be explained by the fact that the bottom PV receives more solar irradiation than the top one given that the aperture of the receiver is lower than the aperture of the space between the receiver and the down edge of the reflector, while this radiation is concentrated in a much narrower region than in the top PV. In the last aperture, solar irradiation hits only the reflector and is directed to

the bottom PV. The concentration of solar irradiation on a very narrow region is the main reason for the bottom PV overheating, since when such a concentration exists, the heat has fewer paths to reach the fluid and thus less fluid volume is utilized for discharging the receiver. It is interesting to note that the temperature difference between the PV and the inlet temperature is greater in low inlet temperatures and can even reach 7 °C. This happens because of the thermal losses variation and for that reason the trend of the curves in Figure 12 is similar to the respective curves of Figure 11. In other words, there is a reduction in useful energy when going to higher inlet temperatures. In particular, the useful energy could be described as the product of the convective heat-transfer coefficient inside the flow channels with the wall's area and the difference between the wall's temperature and the mean water temperature. Considering that the convective regime gets more intense when the inlet temperature increases, the wall temperatures should converge with the mean water temperature. This explains, in an analytical way, why PVs temperatures are getting closer to the inlet temperature with the increase in the mean water temperature.

Figure 13 offers an interesting illustration from the PVs temperature fields on the examined collector for the operating point of 60 °C inlet temperature.

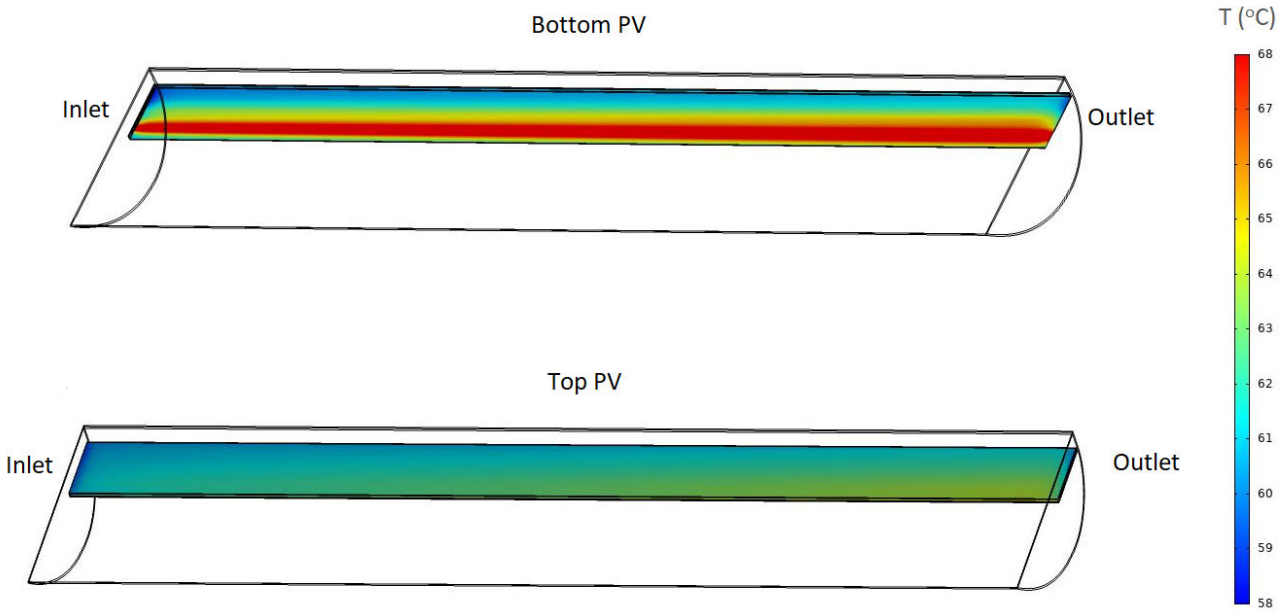

Figure 13. Temperature allocations of the top and the bottom PV of the receiver for $T_{f,i}$ = 60 °C.

It is remarkable to observe from Figure 13 that the temperature fields of the bottom PV are higher than the respective temperature of the top PV. In particular, the maximum temperature at the bottom exceeds 68 °C, while the respective temperature at the top side hardly reaches 64 °C. This happens due to the fact that solar irradiation is concentrated around a narrow region on the bottom PV, while in the top PV, solar irradiation falls uniformly. Another reason for this difference is that the greatest part of the incoming solar irradiation hits the reflector and it ends up on the bottom PV. It is interesting, also, to observe the variation of the temperature allocation on the two PVs in the width direction. More specifically, the temperature appears to take its highest values near the free edge of the receiver on the bottom PV. This occurs because of the reflector's design and especially because the focal line of the reflector is located near the free edge of the receiver on the bottom PV. This variation appears on the top PV too and that is because of thermal coupling between the two PVs through the aluminum hydro-skeleton. Generally, the temperature fields appear to weaken going from the outlet to the inlet of the collector, which is reasonable.

4. Conclusions

A hybrid photovoltaic/thermal (PV/T) solar collector with asymmetric concentrator was examined in this work while its thermal and optical operation was investigated in depth. The following concluding remarks provide a brief summary of the most significant aspects investigated in the present work.

- The ray-tracing results were verified by applying three different programs (Tonatiuh, COMSOL, and SolidWorks) with average deviations lower than 4% among the solutions.
- A novel modeling method was proposed regarding the thermal analysis part and its validity was evaluated by applying it via two different packages (COMSOL and SolidWorks) and comparing it with experimental data. The results indicated that the simulation values were very close to the experimental ones, with maximum deviations lower than 10%, while the two simulation tools obtained similar results with 6.15% maximum declination between each other. Hence, the proposed modeling method was both validated and verified.
- The proposed modeling method ensures sustainability, since it provides the desirable results with lighter computational domain than conventional CFD models, considering that it does not solve the air function at the interior of the gap space, but it takes into consideration the effect of the air presence by an alternative way.
- Through the method proposed it was possible to determine the optimum inclination angle of the collector for each one of the examined months, while it was revealed that the optimum value for the inclination angle decreases going from March to June and increases from June to September.
- The optimization of the tilt angle in each examined case ensures the maximum possible enhancement of the overall performance of the collector, rendering it more sustainable.
- A significant point to mention was that the optimum inclination angle remained constant around a solar time range between 10:00 and 14:00, almost for each month.
- Another important thing to mention is that the examined collector obtains a sufficient thermal efficiency of up to 63% considering an operation between 20 °C and 80 °C inlet temperature. The optical efficiency reaches 76% at optimum tilt angles.
- The electrical output was found to decrease with the increment of the inlet temperature, due to the fact that the PVs temperature increases too.

Generally, it could be stated that the proposed modeling method appears to be reliable and valid considering the comparison with the experimental results, while it offers the opportunity to investigate the thermal operation of the collector by ensuring low computational cost (sustainable solution), given that the enclosed air gap was simulated indirectly. Moreover, the optimal tilt angle determination in each examined case revealed how to utilize the examined collector in the most sustainable way.

Author Contributions: Conceptualization, D.N.K. and T.P.; Methodology, D.N.K. and T.P.; Software, D.N.K. and T.P.; Validation, D.N.K. and T.P.; Formal Analysis, D.N.K. and T.P.; Investigation, D.N.K. and T.P.; Resources, I.K. and C.T.; Writing—Original Draft Preparation, D.N.K. and T.P.; Writing—Review & Editing, I.K. and C.T.; Visualization, D.N.K. and T.P.; Supervision, I.K. and C.T.; Project Administration, I.K. and C.T. All authors have read and agreed to the published version of the manuscript.

Funding: The first author would like to thank the Bodossaki Foundation for its financial support in his post-doctoral research.

Institutional Review Board Statement: Not applicable.

Informed Consent Statement: Not applicable.

Data Availability Statement: Available after request.

Acknowledgments: The authors extend their appreciation, the first author would like to thank the Bodossaki Foundation for its financial support in his post-doctoral research.

Conflicts of Interest: The authors declare no conflict of interest.

Nomenclature

General Parameters

A	Surface area, m^2
Cp	Fluid specific heat, kJ/(kg K)
G	Solar irradiation, W/m^2
h	Heat convection coefficient, $W/(m^2 K)$
L	Length, m
m	Mass flow rate, m^2/s
P	Power, W
Q	Energy rate, W
T	Temperature, °C
u	Wind speed, m/s
V	Volume flow rate, m^3/s

Greek symbols

β	Temperature coefficient of PV cell, %/K
δ	Declination, °
η	Efficiency
θ	Incident angle, °

Dimensionless numbers

C	Concentration ratio

Abbreviations

ACPC	Asymmetric Compound Parabolic Collector
CFD	Computational Fluid Dynamics
CPC	Compound Parabolic Collectors
ETC	Evacuated Tube Collector
FPC	Flat Plate Collector
IAM	Incident Angle Modifier
PTC	Parabolic Trough Collectors
PV/T	Photovoltaic/Thermal
STC	Standard Test Conditions

Subscripts

a	Ambient
abs	Absorbed
b	Beam
bot	Bottom
c	Collector
cpc	Utilized by the reflector
d	Diffuse
eff	Effective
el	Electrical
f	Fluid
i	Inlet
losses	Losses
max	Maximum
n	Normal
o	Outlet
opt	Optical
out	Outside
pv	Photovoltaic
r	Receiver
ref	Reference
s	Solar
sky	Sky
T	Perpendicular to aperture
th	Thermal
top	Top
u	Useful

References

1. Kalogirou, S.A. Solar Thermal Collectors and Applications. *Prog. Energy Combust. Sci.* **2004**, *30*, 231–295. [CrossRef]
2. Kalogirou, S.A. Flat-Plate Collector Construction and System Configuration to Optimize the Thermosiphonic Effect. *Renew. Energy* **2014**, *67*, 202–206. [CrossRef]
3. Korres, D.; Tzivanidis, C. Thermal Analysis of a Serpentine Flat Plate Collector and Investigation of the Flow and Convection Regime. *Therm. Sci.* **2019**, *23*, 47–59. [CrossRef]
4. Subiantoro, A.; Ooi, K.T. Analytical Models for the Computation and Optimization of Single and Double Glazing Flat Plate Solar Collectors with Normal and Small Air Gap Spacing. *Appl. Energy* **2013**, *104*, 392–399. [CrossRef]
5. Wang, D.; Fan, B.; Chen, Y.; Han, Y.; Liu, Y.; Wang, Y.; Liu, H.; Jiao, X. Comparative Analysis of Heat Loss Performance of Flat Plate Solar Collectors at Different Altitudes. *Sol. Energy* **2022**, *244*, 490–506. [CrossRef]
6. He, Q.; Zeng, S.; Wang, S. Experimental Investigation on the Efficiency of Flat-Plate Solar Collectors with Nanofluids. *Appl. Therm. Eng.* **2015**, *88*, 165–171. [CrossRef]
7. Valenzuela, L.; López-Martín, R.; Zarza, E. Optical and Thermal Performance of Large-Size Parabolic-Trough Solar Collectors from Outdoor Experiments: A Test Method and a Case Study. *Energy* **2014**, *70*, 456–464. [CrossRef]
8. Tzivanidis, C.; Bellos, E.; Korres, D.; Antonopoulos, K.A.; Mitsopoulos, G. Thermal and Optical Efficiency Investigation of a Parabolic Trough Collector. *Case Stud. Therm. Eng.* **2015**, *6*, 226–237. [CrossRef]
9. Zou, B.; Yang, H.; Yao, Y.; Jiang, Y. A Detailed Study on the Effects of Sunshape and Incident Angle on the Optical Performance of Parabolic Trough Solar Collectors. *Appl. Therm. Eng.* **2017**, *126*, 81–91. [CrossRef]
10. Shajan, S.; Baiju, V. Designing a Novel Small-Scale Parabolic Trough Solar Thermal Collector with Secondary Reflector for Uniform Heat Flux Distribution. *Appl. Therm. Eng.* **2022**, *213*, 118660. [CrossRef]
11. Xu, L.; Wang, Z.; Li, X.; Yuan, G.; Sun, F.; Lei, D. Dynamic Test Model for the Transient Thermal Performance of Parabolic Trough Solar Collectors. *Sol. Energy* **2013**, *95*, 65–78. [CrossRef]
12. Su, Z.; Gu, S.; Vafai, K. Modeling and Simulation of Ray Tracing for Compound Parabolic Thermal Solar Collector. *Int. Commun. Heat Mass Transf.* **2017**, *87*, 169–174. [CrossRef]
13. Santos-González, I.; García-Valladares, O.; Ortega, N.; Gómez, V.H. Numerical Modeling and Experimental Analysis of the Thermal Performance of a Compound Parabolic Concentrator. *Appl. Therm. Eng.* **2017**, *114*, 1152–1160. [CrossRef]

14. Tchinda, R. Thermal Behaviour of Solar Air Heater with Compound Parabolic Concentrator. *Energy Convers. Manag.* **2008**, *49*, 529–540. [CrossRef]
15. Antonelli, M.; Francesconi, M.; Di Marco, P.; Desideri, U. Analysis of Heat Transfer in Different CPC Solar Collectors: A CFD Approach. *Appl. Therm. Eng.* **2016**, *101*, 479–489. [CrossRef]
16. Korres, D.; Bellos, E.; Tzivanidis, C. Investigation of a Nanofluid-Based Compound Parabolic Trough Solar Collector under Laminar Flow Conditions. *Appl. Therm. Eng.* **2019**, *149*, 366–376. [CrossRef]
17. Korres, D.N.; Tzivanidis, C. A Novel Asymmetric Compound Parabolic Collector under Experimental and Numerical Investigation. *Renew. Energy* **2022**, *199*, 1580–1592. [CrossRef]
18. Korres, D.N.; Tzivanidis, C.; Koronaki, I.P.; Nitsas, M.T. Experimental, Numerical and Analytical Investigation of a U-Type Evacuated Tube Collectors' Array. *Renew. Energy* **2019**, *135*, 218–231. [CrossRef]
19. Nitsas, M.T.; Koronaki, I.P. Experimental and Theoretical Performance Evaluation of Evacuated Tube Collectors under Mediterranean Climate Conditions. *Therm. Sci. Eng. Prog.* **2018**, *8*, 457–469. [CrossRef]
20. Ismail, K.A.R.; Teles, M.P.R.; Lino, F.A.M. Comparative Analysis of Eccentric Evacuated Tube Solar Collector with Circular and Rectangular Absorber Working with Nanofluid. *Clean. Eng. Technol.* **2021**, *3*, 100105. [CrossRef]
21. Li, G.; Xuan, Q.; Lu, Y.; Pei, G.; Su, Y.; Ji, J. Numerical and Lab Experiment Study of a Novel Concentrating PV with Uniform Flux Distribution. *Sol. Energy Mater. Sol. Cells* **2018**, *179*, 1–9. [CrossRef]
22. Renzi, M.; Egidi, L.; Comodi, G. Performance Analysis of Two 3.5 KWp CPV Systems under Real Operating Conditions. *Appl. Energy* **2015**, *160*, 687–696. [CrossRef]
23. Sangani, C.; Solanki, C. Experimental Evaluation of V-Trough (2 Suns) PV Concentrator System Using Commercial PV Modules. *Sol. Energy Mater. Sol. Cells* **2007**, *91*, 453–459. [CrossRef]
24. Tripanagnostopoulos, Y.; Souliotis, M.; Battisti, R.; Corrado, A. Energy, Cost and LCA Results of PV and Hybrid PV/T Solar Systems. *Prog. Photovolt. Res. Appl.* **2005**, *13*, 235–250. [CrossRef]
25. Herrando, M.; Markides, C.N.; Hellgardt, K. A UK-Based Assessment of Hybrid PV and Solar-Thermal Systems for Domestic Heating and Power: System Performance. *Appl. Energy* **2014**, *122*, 288–309. [CrossRef]
26. Herrando, M.; Simón, R.; Guedea, I.; Fueyo, N. The Challenges of Solar Hybrid PVT Systems in the Food Processing Industry. *Appl. Therm. Eng.* **2021**, *184*, 116235. [CrossRef]
27. Jonas, D.; Lämmle, M.; Theis, D.; Schneider, S.; Frey, G. Performance Modeling of PVT Collectors: Implementation, Validation and Parameter Identification Approach Using TRNSYS. *Sol. Energy* **2019**, *193*, 51–64. [CrossRef]
28. Lämmle, M.; Hermann, M.; Kramer, K.; Panzer, C.; Piekarczyk, A.; Thoma, C.; Fahr, S. Development of Highly Efficient, Glazed PVT Collectors with Overheating Protection to Increase Reliability and Enhance Energy Yields. *Sol. Energy* **2018**, *176*, 87–97. [CrossRef]
29. Lämmle, M.; Kroyer, T.; Fortuin, S.; Wiese, M.; Hermann, M. Development and Modelling of Highly-Efficient PVT Collectors with Low-Emissivity Coatings. *Sol. Energy* **2016**, *130*, 161–173. [CrossRef]
30. Herrando, M.; Ramos, A.; Zabalza, I.; Markides, C.N. A Comprehensive Assessment of Alternative Absorber-Exchanger Designs for Hybrid PVT-Water Collectors. *Appl. Energy* **2019**, *235*, 1583–1602. [CrossRef]
31. Guarracino, I.; Mellor, A.; Ekins-Daukes, N.J.; Markides, C.N. Dynamic Coupled Thermal-and-Electrical Modelling of Sheet-and-Tube Hybrid Photovoltaic/Thermal (PVT) Collectors. *Appl. Therm. Eng.* **2016**, *101*, 778–795. [CrossRef]
32. Nasseriyan, P.; Afzali Gorouh, H.; Gomes, J.; Cabral, D.; Salmanzadeh, M.; Lehmann, T.; Hayati, A. Numerical and Experimental Study of an Asymmetric CPC-PVT Solar Collector. *Energies* **2020**, *13*, 1669. [CrossRef]
33. Koronaki, I.P.; Nitsas, M.T. Experimental and Theoretical Performance Investigation of Asymmetric Photovoltaic/Thermal Hybrid Solar Collectors Connected in Series. *Renew. Energy* **2018**, *118*, 654–672. [CrossRef]
34. Proell, M.; Osgyan, P.; Karrer, H.; Brabec, C.J. Experimental Efficiency of a Low Concentrating CPC PVT Flat Plate Collector. *Sol. Energy* **2017**, *147*, 463–469. [CrossRef]
35. Nilsson, J.; Håkansson, H.; Karlsson, B. Electrical and Thermal Characterization of a PV-CPC Hybrid. *Sol. Energy* **2007**, *81*, 917–928. [CrossRef]
36. Bellos, E.; Korres, D.N.; Tzivanidis, C. Investigation of a Compound Parabolic Collector with a Flat Glazing. *Sustainability* **2023**, *15*, 4347. [CrossRef]
37. Christodoulaki, R.; Tsekouras, P.; Koronaki, I. On the Optical Performance of a Spherical Stationary Reflector/Tracking Absorber Solar Collector. *Int. J. Sustain. Energy* **2022**, *41*, 1–11. [CrossRef]
38. Korres, D.N.; Bellos, E.; Tzivanidis, C. Integration of a Linear Cavity Receiver in an Asymmetric Compound Parabolic Collector. *Energies* **2022**, *15*, 8635. [CrossRef]
39. Blanco, M.J.; Mutuberria, A.; Garcia, P.; Gastesi, R.; Martin, V. Preliminary Validation of Tonatiuh. In Proceedings of the SolarPACES 2009 International Conference, Berlin, Germany, 15–18 September 2009; Volume 1, p. 2009.
40. Afzali Gorouh, H.; Salmanzadeh, M.; Nasseriyan, P.; Hayati, A.; Cabral, D.; Gomes, J.; Karlsson, B. Thermal Modelling and Experimental Evaluation of a Novel Concentrating Photovoltaic Thermal Collector (CPVT) with Parabolic Concentrator. *Renew. Energy* **2022**, *181*, 535–553. [CrossRef]
41. COMSOL. *COMSOL Multiphysics Reference Manual*; COMSOL AB: Stockholm, Sweden, 2015.
42. Miao, R.; Hu, X.; Yu, Y.; Zhang, Y.; Wood, M.; Olson, G.; Yang, H. Evaluation of Cooling Performance of a Novel Dual-Purpose Solar Thermal Collector through Numerical Simulations. *Appl. Therm. Eng.* **2022**, *204*, 117966. [CrossRef]

43. Chandan; Suresh, V.; Iqbal, S.M.; Reddy, K.S.; Pesala, B. 3-D Numerical Modelling and Experimental Investigation of Coupled Photovoltaic Thermal and Flat Plate Collector. *Sol. Energy* **2021**, *224*, 195–209. [CrossRef]
44. Hassanzadeh, A.; Jiang, L.; Winston, R. Coupled Optical-Thermal Modeling, Design and Experimental Testing of a Novel Medium-Temperature Solar Thermal Collector with Pentagon Absorber. *Sol. Energy* **2018**, *173*, 1248–1261. [CrossRef]
45. Dassault Systems. *Technical Reference Solidworks Flow Simulation 2015*; Dassault Systems: Dearborn, MI, USA, 2015.
46. Bellos, E.; Tzivanidis, C. Investigation of a Star Flow Insert in a Parabolic trough Solar Collector. *Appl. Energy* **2018**, *224*, 86–102. [CrossRef]
47. Bellos, E.; Tzivanidis, C.; Antonopoulos, K.A.; Gkinis, G. Thermal Enhancement of Solar Parabolic Trough Collectors by Using Nanofluids and Converging-Diverging Absorber Tube. *Renew. Energy* **2016**, *94*, 213–222. [CrossRef]
48. Bellos, E.; Mathioulakis, E.; Tzivanidis, C.; Belessiotis, V.; Antonopoulos, K.A. Experimental and Numerical Investigation of a Linear Fresnel Solar Collector with Flat Plate Receiver. *Energy Convers. Manag.* **2016**, *130*, 44–59. [CrossRef]
49. Huld, T.; Müller, R.; Gambardella, A. A New Solar Radiation Database for Estimating PV Performance in Europe and Africa. *Sol. Energy* **2012**, *86*, 1803–1815. [CrossRef]
50. Technical Chamber of Greece. *Greek Regulation for Buildings Energy Performance, Technical Notes 20701–3/2010*; Technical Chamber of Greece: Athens, Greece, 2010.
51. Duffie, J.A.; Beckman, W.A. (Eds.) *Solar Engineering of Thermal Process*, 4th ed.; John Wiley: Hoboken, NJ, USA, 2013, ISBN 978-0-470-87366-3.